Analysis of Slow-Wave Instability in Rectangularly Corrugated Cylindrical Waveguide

Y.Takashima,K.Ogura,M.Yamakawa and K.Otubo
Graduate School of Science and Technology,
Niigata University, 950-2181 Japan

Md. R. Amin
Electrical and Electronic Engineering Department,
Rajshahi University of Engineering and Technology,
Rajshahi-6204, Bangladesh

(Received: 29 August 2008 / Accepted: 22 December 2008)

Slow-wave instability in a rectangularly corrugated cylindrical waveguide is analyzed. Fields inside corrugation is expressed by a sum of space harmonics satisfying the boundary conditions at the corrugation wall. The corrugation fields are matched to periodic fields outside the corrugation at the boundary of the two regions. Infinitesimally thin annular electron beam is considered including the three-dimensional perturbations. Effects of space harmonics in the corrugation along with the corrugation depth are examined. Slow cyclotron instability in addition to Cherenkov instability occurs when perturbed motions and modulations of infinitely thin surface are included.

Keywords: rectangularly corrugated cylindrical waveguide, space harmonics, infinitely thin annular beam, boundary condition, Cherenkov instability, slow cyclotron instability, backward wave oscillator

1. Introduction

Slow-wave devices such as backward wave oscillators (BWOs) can be driven by an axially streaming electron beam without initial perpendicular velocity and have been studied extensively as a candidate for high-power microwave sources. In the theoretical studies, the Cherenkov instability due to the longitudinal electron motion has mainly been considered [1]. However, for a finite strength magnetic field, not only the Cherenkov instability but also the slow cyclotron instability can be driven by a linearly streaming electron beam without initial perpendicular velocity [2-4]. The slow cyclotron instability is attributed to the transverse perturbation based on the anomalous Doppler effect. It should be noted that the slow cyclotron instability is essentially different from the fast cyclotron instability due to the normal Doppler effect, which requires an initial perpendicular velocity to the magnetic field.

Three kinds of beam models have been considered; cylindrical solid beam, annular beam with finite thickness and infinitesimally thin annular beam. For a cylindrical solid beam, a new version of self-consistent relativistic field theory is developed, taking three-dimensional perturbations into account [5, 6]. Based on this field theory, detailed analyses of the slow cyclotron instability are presented in Refs. [7, 8]. In the new version of field theory, the effect of the transverse beam perturbation appears as a surface charge at a fixed beam surface. For a finitely thick annular beam, the field theory can be developed applying the same boundary conditions to inside and outside beam boundaries as presented in Ref. [9].

For an infinitesimally thin annular beam, the beam boundary is modulated due to the transverse perturbation of annular surface. Analysis of such beams is quite different from the solid and finite-thick annular cases. A pioneering work can be seen in Ref. [10], which is a non-relativistic linear theory of an interaction of sheet beam with distributed circuit elements. Recently, the slow-wave instability with an infinitesimally thin annular beam are analyzed in Ref. [11], presenting a self-consistent relativistic field theory considering the moving modified boundary surface of beam in a dielectric loaded waveguide.

In slow-wave devices, a slow-wave structure (SWS) is used to reduce the phase velocity of electromagnetic wave. Typical SWS is a periodical metallic waveguide with sinusoidal or rectangular corrugations. Sinusoidal corrugations are used in many high-power BWO experiments since electric fields become strong near sharp corners of rectangular. The electric fields become unacceptably strong in extremely high-power operations above some hundreds of MW. For moderate power level of a few MW or less, the breakdown problem may not be so serious and the rectangular shape may be better for beam-wave coupling than the sinusoidal shape [12].

In this paper, we analyze the slow-wave instability using a rectangularly corrugated cylindrical waveguide. We consider a modulated moving annular sheet of beam.

author's e-mail:f07e093f@mail.cc.niigata-u.ac.jp

Boundary conditions at annular beam are based on the relativistic field theory in Ref.[11]. The electromagnetic fields in the rectangularly corrugated SWS are obtained from the so-called "field matching method". And normal modes of the rectangularly corrugated cylindrical system and the slow-wave instability are numerically analyzed. Unique features of our study are analyses of (1) effects of space harmonics in the corrugation along with the corrugation depth and (2) slow cyclotron instability as well as Cherenkov instability. Our analyses are limited to linear phenomena and nonlinear effects are not described in this paper.

2. Boundary Conditions at Moving Modulated Beam Sheet

We consider a rectangularly corrugated cylindrical waveguide in Fig.1; the corrugation amplitude h, corrugation period z_0, average radius R_0, waveguide minimum radius $R_1=R_0-h$ and maximum radius $R_2=R_0+h$. The cylindrical coordinate system (r, θ, z) is introduced in this study. A guiding magnetic field B_0 is applied in the z-direction. Infinitely thin annular electron beam of the radius R_b propagates in the axial direction inside the waveguide. The DC surface charge density and DC velocity is assumed to be σ_0 and $\boldsymbol{v}_0=(0,0,v_0)$, respectively.

Boundary conditions at a moving boundary with a constant speed $\boldsymbol{v}$ are presented in Refs.[14, 15] and results are summarized here for later use. The surface current density and surface charge density are respectively $\boldsymbol{K}$ and σ. Conditions for the normal components of electric $\boldsymbol{E}$ and magnetic $\boldsymbol{B}$ fields are obtained by applying Gauss's laws to a small cylinder, half in one side and half in the other, and are given by,

$$\varepsilon_0(\boldsymbol{E}_{\mathrm{II}}-\boldsymbol{E}_{\mathrm{I}})\cdot\boldsymbol{n}=\sigma \text{ and } (\boldsymbol{B}_{\mathrm{II}}-\boldsymbol{B}_{\mathrm{I}})\cdot\boldsymbol{n}=0. \quad (1)$$

Here, $\boldsymbol{n}$ is the unit normal vector of the boundary surface and suffix "I (II)" means the side I (II) of the sheet.

For the tangential components of boundary condition, Faraday's and Ampere's laws are applied to the small rectangular closed path C around the boundary surface and are given by,

$$\boldsymbol{t}\cdot\left[\boldsymbol{n}\times\left(\boldsymbol{E}_{\mathrm{II}}-\boldsymbol{E}_{\mathrm{I}}\right)\right]-\left(\boldsymbol{n}\cdot\boldsymbol{v}\right)\left[\boldsymbol{t}\cdot\left(\boldsymbol{B}_{\mathrm{II}}-\boldsymbol{B}_{\mathrm{I}}\right)\right]=0\,, \quad (2)$$

$$\boldsymbol{t}\cdot\left[\boldsymbol{n}\times\left(\boldsymbol{B}_{\mathrm{II}}-\boldsymbol{B}_{\mathrm{I}}\right)\right]+\frac{1}{c^2}\left(\boldsymbol{n}\cdot\boldsymbol{v}\right)\left[\boldsymbol{t}\cdot\left(\boldsymbol{E}_{\mathrm{II}}-\boldsymbol{E}_{\mathrm{I}}\right)\right]=\mu_0\boldsymbol{K}\cdot\boldsymbol{t}\,. \quad (3)$$

The different feature of our boundary from Refs. [14, 15] is the fact that the moving boundary is modulated due to the perturbation perpendicular to the boundary surface. We consider a linearized case [11]; $\boldsymbol{v}=\boldsymbol{v}_0+\boldsymbol{v}_1$, $\sigma=\sigma_0+\sigma_1$ and $\boldsymbol{K}=\boldsymbol{K}_0+\boldsymbol{K}_1$. Here, σ_1 is perturbed surface charge, $\boldsymbol{v}_1=(v_{1r},v_{1\theta},v_{1z})$ is the three-dimensionally perturbed velocity, $\boldsymbol{K}_0=(0,0,\sigma_0v_0)$ is DC surface current and $\boldsymbol{K}_1$ is perturbed surface current. The first order velocity $\boldsymbol{v}_1$ can be expressed by the first order electromagnetic fields from the linearized relativistic equation of electron motion under small signal conditions and Maxwell's equations. The tangential components $v_{1\theta}$ and v_{1z} cause the first order surface quantities $\boldsymbol{K}_1$ and σ_1, which are related by the continuity equation on the sheet.

Note that $\boldsymbol{K}_1$ is two-dimensional quantity from the definition; $\boldsymbol{K}_1=(0, \sigma_0v_{1\theta}, \sigma_0v_{1z})$ in our linear theory. The radial velocity v_{1r} causes the radial displacement r_1, resulting in the annular sheet modulation from R_b to R_b+r_1 ($R_b>>r_1$). When the first order inclination angles are δ_θ in the r-θ plane and δ_z in r-z plane, the normal vector $\boldsymbol{n}$ inclines from $\boldsymbol{n}=\boldsymbol{n}_0$ to $\boldsymbol{n}=\boldsymbol{n}_0+\boldsymbol{n}_1$ to the first order. Here, $\boldsymbol{n}_0=(1, 0, 0)$ and $\boldsymbol{n}_1=(0, \delta_\theta, -\delta_z)$.

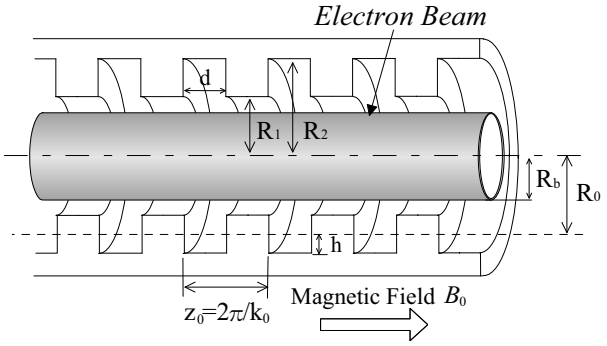

Fig. 1. Model of rectangularly corrugated SWS and annular beam system.

3. Dispersion Relation

The temporal and spatial phase factor of all perturbed quantities is assumed to be $\exp[i(k_zz+m\theta-\omega t)]$. Here, m is the azimuthal mode number, k_z is the axial wave number and ω is the angular frequency. Since the inner wall of the SWS in Fig.1 is spatially periodic, the fields inside the structure are expanded in Floquet's harmonic series. The components of the axial electromagnetic field inside the beam (region I, $r<R_b$) may be expressed as

$$E_{1z}^{\mathrm{I}}=\sum_{p=-\infty}^{\infty}A_{Ep}J_m\left(x_pr\right)$$

$$B_{1z}^{\mathrm{I}}=\sum_{p=-\infty}^{\infty}\frac{\mathrm{i}}{\mathrm{c}}A_{Bp}J_m\left(x_pr\right). \quad (4)$$

And the outside the beam in the waveguide (region II, $R_1>r>R_b$),

$$E_{1z}^{\mathrm{II}}=\sum_{p=-\infty}^{\infty}\left[D_pJ_m\left(x_pr\right)+E_pN_m\left(x_pr\right)\right],$$

$$B_{1z}^{\mathrm{II}}=\sum_{p=-\infty}^{\infty}\frac{\mathrm{i}}{c}\left[F_pJ_m\left(x_pr\right)+G_pN_m\left(x_pr\right)\right]. \quad (5)$$

Here, J_m and N_m are respectively the mth order Bessel function of the first kind and the second kind, $k_p=k_z+pk_0$, p is Floquet's harmonic number and

$$x_p{}^2 = \frac{\omega^2}{c^2} - k_p{}^2 . \qquad (6)$$

The constants A_{Ep}, $A_{Bp,}$ D_p, E_p F_p and G_p are the electromagnetic field coefficients of the vacuum regions. In the rectangular corrugation (region III, $R_2>r>R_1$),

$$E_{1z}^{\mathrm{III}} = \sum_{L=0}^{\infty}[d_L S_m^D\left(\beta_L^E r, \beta_L^E R_2\right)\cos\eta_L^E z - ie_L S_m^D\left(\beta_L^O r, \beta_L^O R_2\right)\sin\eta_L^O z] \qquad (7)$$

$$B_{1z}^{\mathrm{III}} = \frac{\mathrm{i}}{c}\sum_{L=0}^{\infty}[f_L R_m^D\left(\beta_L^O r, \beta_L^O R_2\right)\cos\eta_L^O z - \mathrm{i}g_L R_m^D\left(\beta_L^E r, \beta_L^E R_2\right)\sin\eta_L^E z \qquad (8)$$

Here, d_L, $e_L f_L$ and g_l are constants and

$$\eta_L^E = \frac{2L}{d}\pi\ ,\ \ \eta_L^O = \frac{2L+1}{d}\pi\ , \qquad (9)$$

$$\left(\beta_L^O\right)^2 = \frac{\omega^2}{c^2} - \left(\eta_L^O\right)^2\ ,\ \ \left(\beta_L^E\right)^2 = \frac{\omega^2}{c^2} - \left(\eta_L^E\right)^2 . \qquad (10)$$

And,

$$S_m^D\left(\beta r, \beta R_2\right) = J_m\left(\beta r\right)N_m\left(\beta R_2\right) - J_m\left(\beta R_2\right)N_m\left(\beta r\right) \qquad (11)$$

$$R_m^D\left(\beta r, \beta R_2\right) = J_m\left(\beta r\right)N_m{}'\left(\beta R_2\right) - J_m{}'\left(\beta R_2\right)N_m\left(\beta r\right) \qquad (12)$$

The other field components can be derived from E_{1z} and B_{1z}. The fields inside corrugation given by eqs.(7) and (8) are a sum of standing wave and satisfy the boundary conditions at the rectangular corrugation wall. The normal modes of the system can be derived subject to the given boundary conditions.

From the linearized boundary conditions of (1)-(3) at the moving and modulated beam surface ($r=R_b$), we obtain the four independent equations. Those are for the two tangential components of electric field, the axial component of magnetic field and the radial component of the electric flux density. From these conditions, the constants D_p, E_p F_p and G_p of region II are expressed by the constants A_{Ep} and A_{Bp} of region I.

The fields inside corrugation (region III) are matched to the periodic functions of region II at $r=R_1$. The field matching condition is given by [13],

$$\int_{-z_0/2}^{z_0/2} E_z^{\mathrm{II}}\exp\left(-\mathrm{i}k_q z\right)\mathrm{d}z = \int_{-z_0/2}^{z_0/2} E_z^{\mathrm{III}}\exp\left(-\mathrm{i}k_q z\right)\mathrm{d}z\ , \qquad (13)$$

$$\int_{-z_0/2}^{z_0/2} E_\theta^{\mathrm{II}}\exp\left(-\mathrm{i}k_q z\right)\mathrm{d}z = \int_{-z_0/2}^{z_0/2} E_\theta^{\mathrm{III}}\exp\left(-\mathrm{i}k_q z\right)\mathrm{d}z\ , \qquad (14)$$

$$\int_{-d/2}^{d/2} B_z^{\mathrm{II}}\cos\eta_L^O z\mathrm{d}z = \int_{-d/2}^{d/2} B_z^{\mathrm{III}}\cos\eta_L^O z\mathrm{d}z\ , \qquad (15)$$

$$\int_{-d/2}^{d/2} B_z^{\mathrm{II}}\sin\eta_L^E z\mathrm{d}z = \int_{-d/2}^{d/2} B_z^{\mathrm{III}}\sin\eta_L^E z\mathrm{d}z\ , \qquad (16)$$

$$\int_{-d/2}^{d/2} B_\theta^{\mathrm{II}}\cos\eta_L^E z\mathrm{d}z = \int_{-d/2}^{d/2} B_\theta^{\mathrm{III}}\cos\eta_L^E z\mathrm{d}z\ , \qquad (17)$$

$$\int_{-d/2}^{d/2} B_\theta^{\mathrm{II}}\sin\eta_L^O z\mathrm{d}z = \int_{-d/2}^{d/2} B_\theta^{\mathrm{III}}\sin\eta_L^O z\mathrm{d}z\ . \qquad (18)$$

The conditions (15)-(18) correlate the constants d_L, $e_L f_L$ and g_l of region III with the constants D_p, E_p F_p and G_p of region II. Together with the conditions at the beam, electromagnetic fields in all regions of rectangularly corrugated cylindrical waveguide are expressed in terms of A_{Ep} and A_{Bp} of region I. And then, eqs. (13) and (14) can be expressed in a matrix form as,

$$\begin{bmatrix} \mathrm{D}^{(\mathrm{Z}+)} \mathrm{D}^{(\mathrm{Z}-)} \\ \mathrm{D}^{(\mathrm{T}+)} \mathrm{D}^{(\mathrm{T}-)} \end{bmatrix} \cdot \begin{bmatrix} \mathbf{A}_E \\ \mathbf{A}_B \end{bmatrix} = 0 \qquad (19)$$

Here, $\mathbf{A}_E$ and $\mathbf{A}_B$ are column vectors with elements A_{Ep} and A_{Bp}, and $\mathrm{D}^{(\mathrm{Z}\pm)}$ and $\mathrm{D}^{(\mathrm{T}\pm)}$ are matrixes of an infinite rank. The dispersion relation is obtained from the condition that eq. (19) has a nontrivial solution. After restricting the space harmonics to a finite number, the dispersion relation is given by,

$$\det\begin{bmatrix} \mathrm{D}^{(\mathrm{Z}+)}(\omega, k_z)\, \mathrm{D}^{(\mathrm{Z}-)}(\omega, k_z) \\ \mathrm{D}^{(\mathrm{T}+)}(\omega, k_z)\, \mathrm{D}^{(\mathrm{T}-)}(\omega, k_z) \end{bmatrix} = 0\ . \qquad (20)$$

4. Numerical Result

Figure 2 shows axisymmetric modes without annular electron beam for m=0. Size parameters of SWS are R_0=1.50 cm, z_0=1.67 cm, h=0.25 cm and d/z_0 =0.5. For m=0, $\mathrm{D}^{(\mathrm{Z}-)}$ and $\mathrm{D}^{(\mathrm{T}+)}$ become zero matrices. From the dispersion equation (20), det[$\mathrm{D}^{(\mathrm{Z}+)}$]=0 gives transverse magnetic (TM) modes and det[$\mathrm{D}^{(\mathrm{T}-)}$]=0 gives transverse electric (TE) modes. Pure TM and TE modes are the normal modes in this case. Some of these normal modes (TM_{01}, TE_{01}, TM_{02} and TE_{02}) are presented in Fig.2. The electromagnetic modes in the spatially periodic system are periodic in the wave number space with a period $k_0=2\pi/z_0$. They show band-pass characteristics as can be seen in Fig.2. In order to designate the pass-bands, an index n is introduced. The value of n starts from 1 for the lowest pass-band of each mode as indicated in Fig.2.

TM_{01} is an important fundamental mode for beam interactions based on the slow-wave instability. In Fig.3, an influence of space harmonics in the rectangular corrugation on TM_{01} mode is shown. The dispersion curve moves upward as the number of space harmonics in the corrugation that are involved in eqs. (7) and (8) increases. As can be seen in

eqs.(7) and (8), these space harmonics are standing waves with the axial wave number η_L^E and η_L^O. They are added from L= 0 in sequence. Refer to Fig. 3, the number is "1" means only one standing wave with η_0^E=0. The number "2" means two standing waves with η_0^E=0 and η_0^O=(1/d)π: "3" means three with η_0^E=0, η_0^O=(1/d)π and η_1^E=(2/d)π and "4" means four withη_0^E=0, η_0^O=(1/d)π and η_1^E=(2/d)π andη_1^O=(3/d)π. In Fig. 3, the dispersion curves converge to some extent with five or six space harmonics. The space harmonics with η_L^E have a greater influence than those of η_L^O.

In Fig.4, the dispersion curves for various values of corrugation depth h are shown. The average radius is kept constant value of R_0=1.50 cm. As the value of corrugation depth h increases, the upper cutoff frequency of the pass-band decreases. The lower cutoff frequency is barely influenced by the corrugation depth that consequently causes the flatness of the dispersion curves as h increases.

When a magnetized electron beam is considered, the vertical motions of electron combine to the TM and TE modes. Hence, the normal modes of the system driven by the magnetized electron beam are become hybrid of TM and TE modes even for the axisymmetric case. In order to designate the hybrid modes, two letters of EH and HE are commonly used. However, the definition of EH and HE is rather arbitrary. In this work, the definition in the field of the plasma physics is used [5, 9, 11]. Qualitatively, TM is dominant in EH mode and TE is dominant in HE mode.

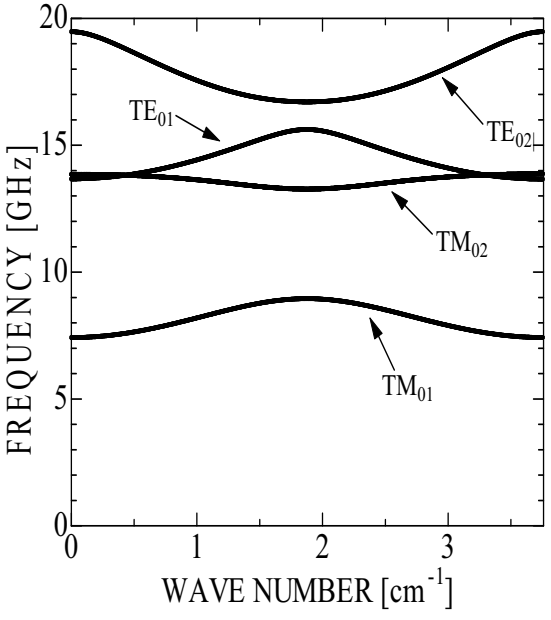

Fig.2. Dispersion characteristics of axisymmetric modes without electron beam. Number of Floquet's harmonics inside the waveguide is seven and number of standing waves in the corrugation is six.

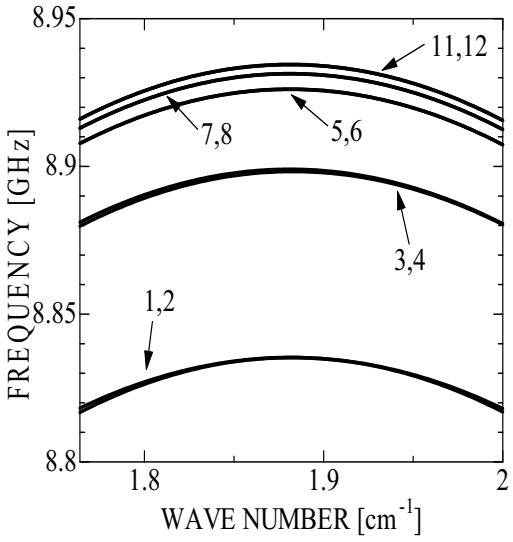

Fig.3. Influence of number of spatial harmonic in the rectangular corrugation on dispersion curves. Size parameters of SWS are same as that are used in Fig.3. Number of Floquet's harmonics inside the waveguide is seven.

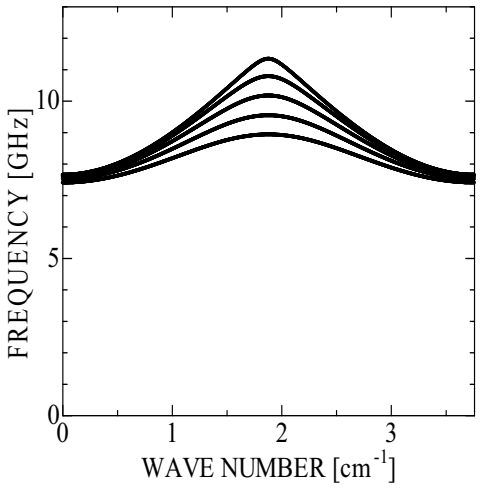

Fig. 4. Influence of the corrugation depth h on the dispersion curve. The arrow in the figure indicates the increasing direction of h. The value of h increases form 0.05 cm to 0.25 cm with a step of 0.05 cm. The other SWS parameters and numbers of spatial harmonics are the same as used in Fig.2.

Figure 5 shows the dispersion curves of EH_{01} mode with the beam energy 430 keV, current 200 A, beam radius R_b=1.00 cm and the magnetic field B_0=0.4 T. The SWS parameters and numbers of spatial harmonics are the same as used in Fig.2. EH_{01} mode becomes TM_{01} without the beam. In the magnetized beam, there are space charge modes, slow cyclotron mode and fast cyclotron mode. The cyclotron modes are attributed to the perpendicular perturbation of

annular beam in the magnetic field, which is taken into consideration in our analysis via the beam boundary. The slow space charge mode is coupled to EH_{01} mode, leading to Cherenkov instability. Slow cyclotron instability occurs due to an interaction of slow cyclotron mode with EH_{01} mode at the location of anomalous Doppler resonance. The temporal growth rates of these instabilities are calculated and the results are shown in the lower frame of Fig. 5. The slow cyclotron instability is much weaker than the Cherenkov instability. The temporal growth rates based on the rectangular corrugation become larger by about 10-20 %, in compared with that of a sinusoidal corrugation with similar dispersion characteristics in X-band. This tendency is also reported for K-band case [12] also.

Note that our treatment is fully relativistic. In our treatment, the surface charge density and surface current density form the four-vector current density (σ/c, $\boldsymbol{K}$). In other words, these quantities in the laboratory frame of reference are transformed to those in the beam fame by the Lorentz transformation. The boundary conditions are also relativistic ones. If the relativity is ignored, the beam velocity becomes larger than the light velocity for the beam of Fig. 5. Moreover, in the non-relativistic case, $v/c \longrightarrow 0$ and the second term on the left side of eq.(3) disappears [14]. The corresponding boundary condition becomes false one and the dispersion characteristics are not studied properly.

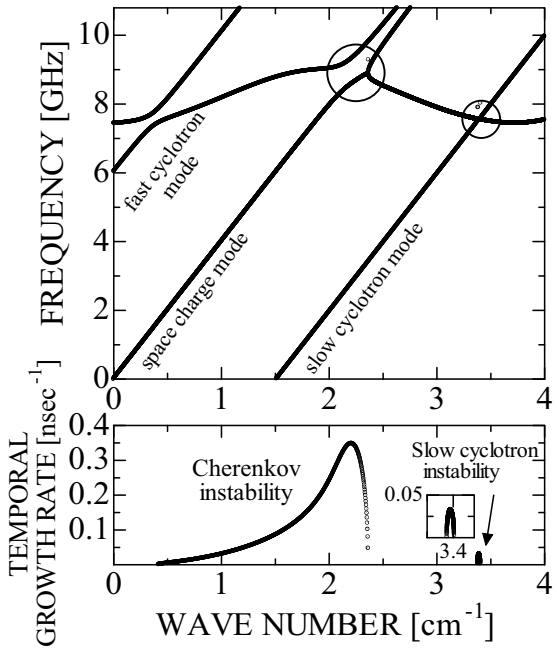

Fig. 5. The dispersion curves of axisymmetric mode (m=0) with beam energy 430 keV, current 200 A, beam radius R_b=1.0 cm and external magnetic field B_0=0.4 T

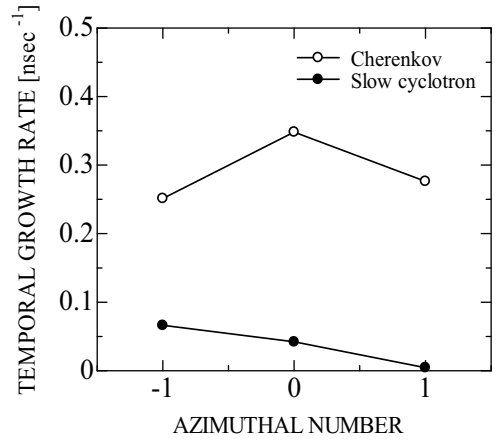

Fig. 6. The temporal growth rate of Cherenkov and slow cyclotron instabilities versus rotational direction of the electromagnetic field.

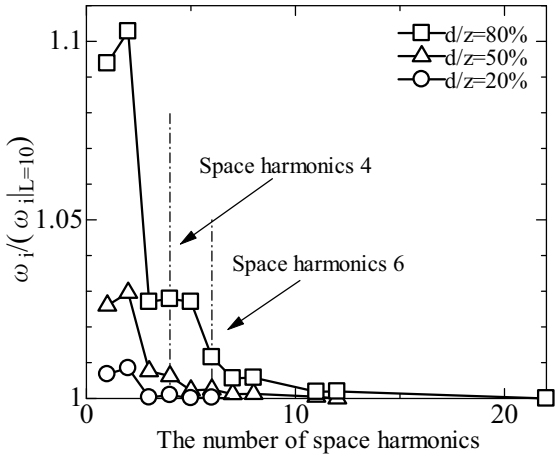

Fig. 7. Cherenkov growth rates as a function of space harmonic number in the corrugation with the corrugation width d/z_0 =0.8, 0.5 and 0.2. Vertical axis is normalized by the temporal growth rate with 22 spatial harmonics in the corrugation.

Figure 6 is the temporal growth rates of slow-wave instabilities versus rotational direction of the electromagnetic wave. The temporal growth rate of the Cherenkov instability is the biggest for m=0. The temporal growth rate of the slow cyclotron instability is the biggest for m=-1. Since the perturbation of $\exp[i(k_z z+m\theta-\omega t)]$ is assumed, the waveguide mode rotates leftward in the laboratory frame of reference .In the beam frame passing the slow-wave, the perturbed cyclotron motion rotates in the same direction as the interacting slow-wave. Hence, the infinitely thin annular beam interact favorably to the nonaxisymmetric mode with m=-1 to produce the slow cyclotron instability.

So far, the dispersion characteristics are calculated with

the corrugation width d/z_0 =0.5. Figure 7 compares numerical results of growth rates of Cherenkov instability by changing the corrugation width ratio d/z_0 as 0.8, 0.5 and 0.2. For d/z_0 =0.8, larger number of spatial harmonics in the corrugation is required to obtain the same convergence as d/z_0 =0.5. It is eleven, compared with five for d/z_0 =0.5. For d/z_0 =0.2, this number is even smaller and is equal to three.

5. CONCLUSION

Slow-wave instability in a rectangularly corrugated cylindrical waveguide is analyzed. Infinitesimally thin annular electron beam is considered taking the three-dimensional perturbations into account. Boundary conditions at the beam are derived by considering a moving modulated surface. The field inside the corrugation is expressed by the sum of standing waves satisfying the boundary conditions at the corrugation wall. The corrugation fields are matched to the periodic fields outside corrugation at the boundary between inside and outside the corrugation. The space harmonics in the rectangular corrugation affect the dispersion characteristics. Fairly convergent results are obtained with five or six space harmonics with the corrugation width of 50 % of the period. The wider width of the corrugation requires the larger number of special harmonics in the corrugation. The frequency of upper cutoff at the π mode decreases with increasing the corrugation depth. Not only Cherenkov instability but also slow cyclotron instability occurs even for the infinitely thin annular beam as long as the three-dimensional perturbed motions are included. The slow cyclotron instability is due to the perpendicular modulation of annular sheet and much smaller than the Cherenkov one. Slow-wave instability for the rectangular corrugation seems stronger by about 10-20 %, in compared with that for the sinusoidal case.

Acknowledgements

This work was partially supported by Grant-in-Aid for Scientific Research from the Ministry of Education, Science, Sports and Culture of Japan, and by NIFS Collaboration Research Program.

REFERENCES

[1] R. J. Barker and E. Schamiloglu, *High-Power Microwave Sources and Technologies*, IEEE Press, NY (2001) Chapter 5.
[2] Md. R. Amin *et al*., J. Phys. Soc. Jpn. **64**, 4473 (1995).
[3] K. Ogura *et al*., Phys. Rev. E **53**, 2726 (1996).
[4] K. Ogura *et al*., J. Phys. Soc. Jpn. **67**, 346 2 (1998).
[5] O. Watanabe *et al*., Phys. Rev. E, **63**, 056503(2001) .
[6] K. Ogura *et al*., Jpn. J. Appl. Phys. **42**,7095 (2003) .
[7] H. Yamazaki *et al*., IEEJ Trans. FM **124**, 477 (2004) .
[8] H. Yamazaki *et al*., IEEJ Trans. FM **125**, 739 (2005).
[9] S. Tamura *et al*., Plasma Fusion Res. **3**, S1020 (2008).
[10] J. R. Pierce, *Traveling-Wave Tube*, Van Nostrand, Toronto (1950) Chapter 13.
[11] K. Ogura *et al*., J. Plasma Phys. **72**, 905 (2006). .
[12] K. Ogura *et al*., IEEJ Trans. FM **127**, 681 (2007) .
[13] P. J. B. Clarricoats and A. D. Olver, *Corrugated Horns for Microwave Antenna*, Peter Peregrinus, London (1984) p.199.
[14] P. D. Noerdlinger, Am. J. Physics **39**, 191(1971).
[15] J. D. Jackson, *Classical Electrodynamics,* 2nd ed., John Wiley & Sons, New York (1975) p.17.